Colloids and Surfaces B: Biointerfaces 177 (2019) 294–305

Contents lists available at ScienceDirect

Colloids and Surfaces B: Biointerfaces

journal homepage: www.elsevier.com/locate/colsurfb

Indocyanine green/doxorubicin-encapsulated functionalized nanoparticles for effective combination therapy against human MDR breast cancer

Hsin-Hung Chen[a], I.-Lin Lu[b,c], Te-I Liu[b], Yuan-Chung Tsai[b], Wen-Hsuan Chiang[a], Sung-Chyr Lin[a,*], Hsin-Cheng Chiu[b,*]

[a] Department of Chemical Engineering, National Chung Hsing University, Taichung, 402, Taiwan
[b] Department of Biomedical Engineering and Environmental Sciences, National Tsing Hua University, Hsinchu, 300, Taiwan
[c] Department of Surgery, Hsinchu Mackay Memorial Hospital, Hsinchu, 300, Taiwan

ARTICLE INFO

Keywords:
Drug delivery nanoparticles
Multidrug resistance
Cholesterol-PEG
Combination chemo/thermal therapy
Synergistic effect

ABSTRACT

To overcome low therapeutic efficacy of chemotherapy against multidrug resistance (MDR) breast cancer, a combination therapy system based upon functionalized polymer nanoparticles comprising poly(γ-glutamic acid)-g-poly(lactic-co-glycolic acid) (γ-PGA-g-PLGA) as the major component was developed. The NPs were loaded with doxorubicin (DOX) and indocyanine green (ICG) for dual modality cancer treatment and coated with cholesterol-PEG (C-PEG) for MDR abrogation in treatment of human MDR breast cancer. The in vitro cellular uptake of the DOX/ICG loaded nanoparticles (DI-NPs) by MDR cancer cells was significantly enhanced owing to effective inhibition of the P-gp activity by C-PEG and γ-PGA receptor-mediated endocytosis. DOX localization in cytoplasm and nucleus was observed particularly with the photo-thermal effect that facilitated intracellular drug release. As a result, the C-PEG coated DI-NPs after photo-irradiation exhibited a synergistic effect of combination (chemo/thermal) therapy to depress the proliferation of MDR cancer calls. The ex vivo biodistribution study revealed an enhanced tumor accumulation of C-PEG (2000) coated DI-NPs in MCF-7/MDR tumor-bearing nude mice due to the excellent EPR effects by the NP surface PEGylation. The MDR tumor growth was almost entirely inhibited in the group receiving combination therapy from CP2k-DI-NPs and photo-irradiation along with substantial cell apoptosis of tumor tissues examined by immunohistochemical staining. The results demonstrate a promising dual modality therapy system, CP2k-DI-NPs, developed in this work for effective combination therapy of human MDR breast cancer.

1. Introduction

Overcoming multidrug resistance (MDR) in chemotherapeutic treatments of malignant tumors remains a major challenge. The development of MDR in cancer cells often associates with the overexpression of ATP-binding cassette (ABC) transporter proteins [1,2]. For example, the permeability glycoprotein (P-gp), responsible for modulating ATP-driven drug efflux from the cytoplasm of MDR cancer cells, encoded by MDR1 gene was often overexpressed on cell membranes [2,3]. Approaches to effectively impairing MDR with P-gp inhibitors, such as verapamil and disulfiram [4,5], and interfering RNAs capable of reducing P-gp expression [6] have been studied. Non-ionic surfactants, such as Pluronic, Tweens, D-alpha tocopheryl polyethylene glycol 1000 succinate (TPGS), PEG/cholesterol adducts, and Brij were also found to reduce drug resistance by disturbing and destabilizing membrane structures [7–11]. Successful deliveries of these MDR-sabotaged agents to tumor sites are essential either to retain structural integrity (activity) and enhance cellular uptake (siRNA) or reduce undesired side effects (P-gp inhibitors and non-ionic membrane-disrupting surfactants) [12–17].

Among various delivery strategies, nanoparticles (NPs)-based carrier systems provide a facile approach for co-delivery of MDR-sabotaged agents with therapeutics as the NP accumulation in tumor sites can be improved via the enhanced permeability and retention (EPR) effects owing to tumor angiogenesis [18,19]. In addition to improved aqueous solubilization of hydrophobic therapeutics by entrapment within dispersible colloids, the NP-based therapy systems can be further functionalized to increase therapeutic efficacy, for example, by decorating with biorecognizable ligands that simultaneously enhances selective delivery to tumors and cellular uptake via receptor-mediated endocytosis. The drug release can be modulated by disrupting/altering NP structure in response to either simple particle degradation or

* Corresponding author.
E-mail addresses: sclin@dragon.nchu.edu.tw (S.-C. Lin), hscchiu@mx.nthu.edu.tw (H.-C. Chiu).

https://doi.org/10.1016/j.colsurfb.2019.02.001
Received 8 October 2018; Received in revised form 22 January 2019; Accepted 2 February 2019
Available online 05 February 2019
0927-7765/

external/internal stimuli [20–22]. For instances, hyaluronic acid (HA) coating on NP surface has been found capable of complementary association with CD44, a cell surface glycoprotein, thus enabling the coated NPs targetable to CD44-overexpressed cells, including macrophages and several cancer cells [23,24]. Similarly, poly(γ-glutamic acid) (γ-PGA) elaborated on NP surfaces was reported to enhance cellular uptake via the binding with γ-glutamyl transferase expressed on cell membranes [25]. Hydrophobic and biodegradable (co)polymers such as ploy(L-lactic acid), poly(L -lactic-co-glycolic acid) (PLGA) and ploy(caprolactone) have also been widely employed as the hydrophobic constituents of polymer micelle-like colloids in the development of polymer NP-based therapeutics delivery systems [23,26,27]. A slow release of nonpolar therapeutics can be attained upon surface degradation (hydrolysis) of these polyesters as the major components of NP. While amphiphilic HA-g-PLGA has been adopted as a CD44 targeted delivery system of therapeutics, the use of copolymers of γ-PGA with PLGA or other similar biodegradable polyesters as functionalized drug carriers for enhanced cellular uptake was barely reported.

Owing to the remarkable progress of various therapeutic modalities, increased attentions have been paid to the combination therapy (such as dual-chemotherapy [28–32] or combined chemo/thermotherapy [33]) and advanced theranostic (therapy + diagnosis [34,35]) strategies in particular in association with the NP-based delivery systems for effective cancer treatments [36]. It has been adopted to combine chemotherapy with either photothermal therapy (PTT) or photodynamic therapy (PDT) for the desired synergistic cancer treatment [21,33]. While the therapeutic effects of both PDT and PTT upon photo-irradiation could lead to a cooperative action with chemotherapy on MDR cancer treatment, the hyperthermia effect may further impair the P-gp activity by thermal ablation of the glycoprotein structure. Photothermal materials such as gold nanorods and indocyanine green (ICG) have been frequently adopted in PTT applications [37–39]. These PTT materials usually exhibit low intrinsic cytotoxicity and are readily induced to produce hyperthermia effect with NIR irradiation. In particular, ICG, an FDA approved fluorescence dye, has been shown to exhibit impressing therapeutic effect in combination with chemotherapy as NP-based dual modality therapy systems to inhibit MDR cancer growth [22,40].

In this work, γ-PGA-g-PLGA and cholesterol-PEG conjugate (C-PEG) were employed to prepare the functionalized NP-based delivery system loaded with DOX and ICG for dual modality treatment of MDR cancers. The loading efficiencies of the active compounds in NPs were determined and the colloidal stability was evaluated by dynamic light scattering (DLS). The in vitro cellular uptake of the DOX/ICG loaded NPs (DI-NPs) by MCF-7/MDR breast cancer cells was examined by laser scanning confocal microscopy. The cell viability of the chemotherapy, the photothermal therapy and the combination therapy was investigated in vitro against MCF-7/MDR cancer cells. The ex vivo biodistribution of C-PEG coated DI-NPs administered intravenously in nude mice bearing MDR breast cancer was examined and the in vivo therapeutic efficacy in terms of the tumor growth inhibition was evaluated.

2. Materials and methods

2.1. Chemicals, drugs and cell lines

PLGA (LA/GA 75/25, Mw 10000 g/mol), monomethoxy-polyethylene glycols (mPEG), *N*-hydroxysuccinimide (NHS), *N,N*'-dicyclohexylcarbodiimide (DCC), 3-(4,5-dimethyl-2-thiazolyl)-2,5-diphenyl-2-tetrazolium bromide (MTT), β-estradiol, Hoechst 33258, and DMSO-d_6 were obtained from Sigma-Aldrich (USA). γ-PGA was purchased from VEDAN (Taiwan). DOX was acquired from Seedchem (Australia). All organic reagents were of analytical grade. Dulbecco's modified Eagle's medium (DMEM), fetal bovine serum (FBS), and 0.25% trypsin–EDTA and penicillin–streptomycin solutions were purchased from Thermo Fisher Scientific (USA). Rabbit anti-mouse caspase-3 antibody and Alexa Fluor 488® goat anti-rabbit antibody were obtained from Abcam (USA). MCF-7 and MCF-7/MDR were obtained from Food Industry Research and Development Institute (Taiwan) and courtesy of Dr. San-Yuan Chen of Department of Materials Science and Engineering at National Chiao Tung University, Taiwan, respectively. Balb/c C57B nude mice were purchased from the National Laboratory Animal Center (Taiwan).

2.2. Synthesis and characterization of cholesterol-PEG derivatives and γ-PGA-g-PLGA

Cholesterol-PEG conjugate (C-PEG) was prepared by dissolution of mPEGs (Mw 2,000, 5,000, or 10,000 g/mol) and cholesteryl chloroformate in a molar ratio of 1:1.1 in dichloromethane in the presence of 4-(dimethylamino) pyridine as the catalyst and the acylation reaction proceed at room temperature for 3 days [41]. The C-PEG was obtained by precipitation from dry ethyl ether. The composition of C-PEG was confirmed by ^{1}H-NMR (Bruker Avance-850NMR Spectrometer) in $CDCl_3$ at ambient temperature. To prepare γ-PGA-g-PLGA, γ-PGA, PLGA, DCC, NHS and DMAP in the molar ratio of 1.0 : 0.15 : 0.5 : 0.2 : 0.5 were mixed in anhydrous DMSO and the reaction was conducted at room temperature for 5 days, as illustrated in Figure S1. After the reaction, N, N'-dicyclohexylurea was removed by repeated filtration. γ-PGA-g-PLGA was purified by dialysis with Cellu-Sep T4 membrane (MWCO 50,000, Membrane Filtration Products, USA) against deionized water for 1 week and collected by lyophilization. The chemical structure and the calculated conversion yield of γ-PGA-g-PLGA were confirmed and determined by ^{1}H-NMR in DMSO-d_6 [42]. The purity was confirmed by gel permeation chromatography (GPC; Agilent 1100 series equipped with PLgel 5 mm, 7.5 mm x 300 mm, Agilent 79911GP-503) using DMSO as the eluent at a flow rate of 1.0 mL/min under RI detection.

2.3. Preparation and characterization of DOX/ICG-loaded nanoparticles (DI-NPs)

DOX in base form was produced by mixing doxorubicin hydrochloride (DOX-HCl) and TEA in a molar ratio of 1:2 in DMSO overnight [43]. The solution thus obtained was used as the stock solution. DOX/ICG-loaded nanoparticles (DI-NPs) were prepared by mixing γ-PGA-g-PLGA (6 mg), C-PEG (C-PEG2k, C-PEG5k, or C-PEG10k, 1.2 mg), DOX base (0.6 mg) and ICG (0.6 mg) in DMSO (0.5 mL) as the organic phase, which was then added dropwise into the phosphate buffer (pH 7.4, ionic strength 10 mM, 3.5 mL) and stirred at room temperature for 1 h. The organic solvent and unencapsulated drugs were subsequently removed from the DI-NPs by dialysis against pH 7.4 phosphate buffer using Cellu-Sep T4 membrane (MWCO 12,000–14,000) at 4 °C for 5 days.

The encapsulation efficiency was determined by the measurements of the fluorescence intensity of DOX and ICG from the DI-NP solution in DMSO using a microplate reader (FLUOstar, OPTIMA, BGM Labtech, Germany) with the excitation wavelength of 480 (780) nm and the emission wavelength of 560 (830) nm for DOX (ICG). The encapsulation efficiency herein was defined as the percentage of DOX/ICG remained in DI-NPs upon dialysis with respect to the amount of DOX/ICG in feed during NP preparation. The loading content was calculated as the ratio of the weight of DOX/ICG in freeze-dried DI-NPs to the weight of freeze-dried DI-NPs. The particle size, polydispersity index (PDI), and zeta potential of the DI-NPs were characterized by dynamic light scattering (DLS, Malvern ZetaSizer Nano Series instrument, USA) with He-Ne laser 4 mW, λ = 633 nm. The morphology of the DI-NPs was examined by transmission electronic microscopy (TEM) conducted on a JEOL JEM-1200 CXII microscope operating at an accelerating voltage of 120 kV. The colloidal stability of DI-NPs was evaluated in terms of the variation of hydrodynamic particle size in DMEM containing 10% FBS over the time periods of 3 and 24 h.

2.4. Drug release of DI-NPs

The drug release profiles of DI-NPs were studied in buffered saline solutions of pH 4.7 (succinate) and 7.4 (phosphate) at 37 °C. DI-NP solution (1 mL) containing 0.5 mg DOX/ICG was subjected to dialysis (Cellu-sep MWCO 12,000–14,000) against 40 mL buffer saline solution (pH 4.7 or 7.4). At the prescribed time intervals, 1 mL outer buffer was withdrawn and the amount of DOX released was quantified by the fluorescence measurements. With each sampling, 1 mL fresh buffered saline was added to the outer aqueous phase. The cumulative DOX release was determined as the ratio of the amount of DOX released to the original amount of DOX encapsulated in the DI-NPs. After 48 h, the ICG in dialysis bag was harvested by lyophilization. The cumulative ICG release was determined as the ratio of the amount of released ICG at 48 h to the initial amount of ICG at 0 h.

2.5. In vitro photothermal effects

To examine the photothermal effect, DI-NPs containing ICG at concentrations of 10 and 20 μM were irradiated with 808 nm laser (0.75 W) for 10 min A thermal camera (Thermo Shot F30) was employed to monitor the temperature of each sample under irradiation.

2.6. In vitro cellular uptake study

MCF-7, MCF-7/MDR, A549 and Hela cancer cells in DMEM containing 10% FBS and 1% penicillin were seeded on a 6-well cell culture plate, at 2×10^6 cancer cells per well, and incubated at 37 °C under 5% CO_2 overnight. Each well was then treated with free DOX-HCl/ICG, free DOX base/ICG, or DI-NPs, with the DOX/ICG concentration of 20/20 μM, for 6 h. The cancer cells were subsequently washed with PBS three times and harvested with trypsin-EDTA. After centrifugation, the DOX fluorescence of cancer cells were determined by flow cytometry (Calibur™).

To evaluate the cellular uptake by laser scanning confocal microscopy (LSCM), cancer cells were seeded on 22 mm glass coverslips placed in a 6-well plate at 5×10^5 cells/well and incubated at 37 °C under 5% CO_2 overnight. The cells were treated with free DOX/ICG or DI-NPs at the DOX/ICG concentration of 20/20 μM for 6 h, and then washed with PBS twice. Cancer cells on the glass coverslips were fixed with 4% PFA and then washed with PBS twice. Nuclei of cancer cells were stained with Hoechst 33258 at 37 °C for 5 min and washed with PBS twice. Cancer cells were then fixed with mounting gel, and the coverslips were covered with microslides. The distribution of DOX within cancer cells were examined by LSCM (ZEISS LSM-780) with an excitation wavelength of 488 nm and an emission wavelength of 560 nm. Hoechst was monitored with an excitation wavelength of 350 nm and an emission wavelength of 480 nm.

To further examine the hyperthermia effect on intracellular distribution and accumulation of DOX within cancer cells by LSCM, MCF-7/MDR cancer cells were treated with free DOX/ICG, DI-NPs (DOX/ICG concentration = 20/20 μM) at 37 °C for 6 h as aforementioned and then irradiated with 808 nm laser (0.75 W/cm^2) for 10 min After irradiation treatment, the cancer cells were re-incubated at 37 °C for extended 6 h. The cancer cells treated only with free DOX/ICG and DI-NPs, respectively, for 12 h without photo-irradiation were employed as the photothermal negative control. With the nuclei being stained with Hoechst 33258, the distribution of DOX within cancer cells was directly visualized by LSCM.

2.7. Cytotoxicity analysis of DI-NPs for combination therapy

MCF-7/MDR cells were seeded into 6-well plates at 2×10^5 cells/well in DMEM (2.0 mL) containing 10% FBS and 1% penicillin, and incubated at 37 °C overnight under 5% CO_2. The cancer cells were treated with free DOX/ICG and DI-NPs at the DOX/ICG concentration of 20/20, 10/10, and 5/5 μM for 6 h. After washing with saline twice, the cancer cells were harvested with trypsin–EDTA and then treated with 808 nm laser (0.75 W/cm^2) for 10 min. The cancer cells were reseeded on 96-well plates at a concentration of 1×10^4 cells in 0.2 mL DMEM per well and incubated at 37 °C under 5% CO_2 for 48 h. To determine the cell viability of cancer cells, MTT (250 μg/mL) in DMEM was added into each well, followed by re-incubation at 37 °C for 2 h. The absorbance of each well at 570 nm was determined by the microplate reader. The MTT assay for the cell viability evaluation was performed based upon the measurement of the cellular metabolic activity, in particular in terms of the activity of mitochondria reductase (dehydrogenase) by colorimetric determination [44]. The cytotoxicity was calculated as % Cytotoxicity = (100 × (Control - Sample))/Control and the cell viability as % Viability = 100% - % Cytotoxicity. For chemotherapy alone, the cancer cells were treated only with free DOX/ICG and DI-NPs, respectively, at the DOX/ICG concentration of 20/20, 10/10, and 5/5 μM for 6 h without further photo-irradiation. After washing with saline twice, the cancer cells were incubated for 48 h and the cell viability was evaluated by MTT assay. To evaluate the in vitro efficacy of PTT alone, the cancer cells were treated with free ICG and I-NPs at the ICG concentration of 20, 10, and 5 μM for 6 h. After washing with saline twice, the cancer cells were harvested with trypsin–EDTA and then irradiated with 808 nm laser (0.75 W) for 10 min. The cancer cells were further incubated for 48 h and the cell viability was determined.

2.8. Biodistribution of DI-NPs

The 7-week-old Balb/c nude mice were purchased from National Laboratory Animal Center, Taiwan. The approved guides for the care and use of laboratory animals by the Institutional Animal Care and Use Committee (IACUC) of National Tsing Hua University, Taiwan (approved number: IACUC:10244) were followed at all times. All surgeries were performed under Zoletil/Rompun anesthesia, and all eff ;orts were made to minimize suff ;ering. Tumors were produced by subcutaneous inoculation of 1×10^6 viable MCF-7/MDR cells in PBS containing 50% matrigel into the right thigh of the mice while being fed with β-estradiol at a concentration of 2 mg/L in daily drinking water to induce the growth of the hormone-dependent MCF-7/MDR cells [45]. The feeding of β-estradiol was terminated 1 week before the DI-NPs administration. The nude mice bearing tumor of the size ~100 mm^3 were injected with free DOX/ICG or DI-NPs at the doses of DOX and ICG of 2.0 and 3.0 mg/kg via the tail vein. The nude mice were sacrificed one day after injection. Tumor and major organs, including heart, liver, spleen, lung, and kidney, were collected for ex vivo ICG distribution examination with an in vivo imaging system (Caliper IVIS Spectrum) with excitation and emission wavelengths at 780 and 830 nm. The organs and tumor harvested were sliced, lyophilized and immersed in anhydrous DMSO for 5 h under stirring. The ICG amount in each organ and tumor was determined by the fluorescence spectrometer in DMSO solution. The size of the tumor herein was evaluated as 0.52× length × width × height [26].

2.9. Tumor inhibition

The MDR tumor model protocol of nude mice was described earlier. In the tumor growth inhibition study, the MDR tumor size of nude mice was allowed to grow to 100 mm^3. The nude mice were treated with free ICG/DOX, DI-NPs, DI-NPs and CP2k-DI-NPs, respectively, at the DOX/ICG dose of 2.0/3.0 mg/kg via intravenous injection. The photothermal activation was performed by NIR irradiation at the wavelength of 808 nm (0.75 W/cm^2) for 10 min at 6 h post-injection. Each group was treated with a total of 5 doses at day 0, 2, 4, 6, and 8. The tumor size and body weight of nude mice were recorded every day to estimate the therapeutic efficacy and side effects of the DI-NPs for a month.

2.10. Immunohistochemistry of Caspase-3

The nude mice bearing MCF-7/MDR tumor were injected intravenously with free DOX/ICG, DI-NPs, or CP2k-DI-NPs. Six hours post-administration, the mice were irradiated with 808 nm laser for 10 min After 48 h, the tumors on the nude mice were harvested for cryo-section. Primary antibody (rabbit anti-mouse caspase-3 antibody) and fluorescence-labeled secondary antibody (Alexa Fluor 488® goat anti-rabbit antibody) were employed for the immunohistochemical (IHC) identification of the apoptosis regions of tumor in the cryo-sections. The cell nuclei were stained with DAPI. All of the stained tumor sections were examined by LSCM with the fluorescence channels for DAPI and Alexa Fluor 488.

2.11. Hematoxylin and eosin staining

Major organs (heart, liver, spleen, lung, and kidney) and tumors were collected on day 30 after the first IV injection treatment, sliced into 5 μm-thick sections on slide, and H&E stained [46]. The tissues were examined using optical microscopy (Olymplus IX70) to estimate the side effect of major organs and therapeutic efficiency.

2.12. Statistical analysis

All experiments were performed in triplets, and data were reported as mean ± standard deviation. Statistical significance was determined using Student's *t*-test. Significant differences were defined as (*) $P < 0.05$ and (**) $P < 0.01$. Not significant differences were displayed as NS ($P > 0.05$).

3. Results and discussion

3.1. Preparation and characterization of γ-PGA-g-PLGA and cholesterol/PEG adducts

The conjugation of cholesterol to PEG with molecular weights ranging from 2,000 to 10,000, via acylation was conducted as reported previously [41]. Based on ^{1}H-NMR spectrum shown in Figure S2, the conversion efficiency of C-PEG, calculated with the areas of PEG (3.30 ppm) and cholesterol (5.37 ppm), was 89.9%. The γ-PGA-g-PLGA was synthesized via the DCC coupling reaction of γ-PGA with PLGA. The ^{1}H-NMR spectrum is shown in Figure S3. The extent of PLGA grafted to γ-PGA with respect to 100 γ-GA residues, calculated with the areas of PLGA (1.45 ppm) and γ-PGA (4.12 ppm), was 12.0%.

To prepare the self-assembly nanoparticles via nanoprecipitation, the amphiphilic γ-PGA-g-PLGA polymer, containing hydrophilic γ-PGA main chain and hydrophobic PLGA grafts, was mixed with C-PEG, DOX and ICG in DMSO, which was then added into the aqueous phase dropwise. Owing to the difference in hydrophilic/hydrophobic nature between DOX-HCl and the micellar core of DI-NPs consisting mainly of PLGA, the relatively hydrophilic DOX-HCl was not effectively encapsulated, with the loading efficiencies < 20%. In addition, the significant burst release behavior of encapsulated DOX-HCl from DI-NPs was **observed (Figure S4), implying** the high possibility to induce side effects to the normal organs and tissues and thus limiting the clinical application of DOX for the treatment of cancers. To enhance the DOX loading efficiency of DI-NPs and reduce the premature release of DOX in blood circulation, DOX in free base form was employed to prepare DI-NPs. The major characteristics of the DI-NPs thus prepared are summarized in Table 1. The particle sizes of DI-NPs with C-PEG coating, ranging from 52 to 58 nm, were slightly larger than that without C-PEG coating (ca 51 nm), because C-PEG coatings have been shown to increase the hydrodynamic diameters of nanoparticles in the aqua phase [47]. Nevertheless, the particle sizes of all the NPs with and without C-PEG coating are within the favored range for the EPR effect, allowing the preferential accumulation of drug in tumor sites [48]. The particle sizes of the DI-NPs under TEM examination (Figure S5) were slightly smaller than 50 nm due to the dehydration of DI-NPs on the TEM carbon support films. The drug loading efficiencies for DOX and ICG were 63.8% to 66.8% and 83.4% to 86.8%, respectively. Taking molecular weights, 543.52 for DOX and 774.96 for ICG, into account, the molar ratios of the DOX to ICG encapsulated in the DI-NPs were essentially equal to 1.0. As shown in Table 1, the drug loading contents of the bare DI-NPs were higher than that of C-PEG-DI-NPs, because the particle mass of DI-NPs was smaller without PEG coating. All the DI-NPs exhibited negative surface charges, which could reduce the interaction with the negatively charged cell membrane and thus the cytotoxicity to normal cells [49]. The particle size distributions of the DI-NPs suspended in DMEM containing 10% FBS are shown in Figure S6. The profiles of the DI-NPs remained unchanged, with a minor peak corresponding to that of FBS proteins, indicating that the DI-NPs did not severely interact with plasma proteins. No aggregation of DI-NPs and plasma proteins was observed for 24 h, indicating that the DI-NPs exhibited high colloidal stability and were suited for clinical applications.

3.2. Drug release behavior

The drug release behaviors of the DI-NPs were studied at pH characteristic of the blood circulation (pH 7.4) with PBS and of the subcellular acidic organelles (4.7) with succinate buffered saline [50]. As shown in Fig. 1, unlike those reported in the literature [51,52], the 48 h cumulative releases of DOX base from the DI-NPs at pH 4.7 were only marginally higher than that at pH 7.4, indicating that the DI-NPs exhibited poor pH-response. This could be attributed to the entrapment of DOX base in the dense hydrophobic core consisting of the PLGA segments of γ-PGA-g-PLGA. As a consequence, slow drug release profiles of the DI-NPs at either pH 7.4 or 4.7 were attained (Fig. 1). Nevertheless, this would not affect the potential clinical applications of the DI-NPs, as the biodegradable materials would be readily disrupted in cancer cells, allowing the release of DOX base.

Although ICG has been approved by FDA (USA) as the diagnostics agent for determining cardiac output, hepatic function, and liver blood flow [53,54], it has a short circulation half-life of ca 3–4 min [55]. To delay the clearance of ICG from blood circulation and enhance its transport to tumor sites via EPR effects, ICG was encapsulated in the DI-NPs. The 48 h accumulated release percentages were relatively low, 25.1% to 31.1% at pH 7.4 over 48 h, demonstrating a significantly reduced premature leakage from the DI-NPs in blood stream (Figure S7). At pH 4.7, a slow ICG release from the DI-NPs, 32.3% to 36.4% for 48 h, was also observed, implying that a better photothermal effect of ICG can be plausibly attained intracellularly by being entrapped within the NPs as shown below.

3.3. In vitro photothermal effect study

To evaluate the photothermal efficiency of ICG, the DI-NPs were irradiated with 808 nm laser (0.75 W/cm^2). The temperature of the solutions of free ICG and DI-NPs at an ICG concentration of 10 μM increased for the first 6 min under 808 nm irradiation (Figure S8A). After that, the solution temperature decreased slowly due to the irreversible decomposition of ICG under the irradiation. While the temperature profiles of the DI-NP groups were essentially identical, the extent of temperature change for the free ICG solution was lower. The maximum temperature rises for the solutions of free ICG and DI-NPs at the ICG concentration of 10 μM were 9.3 ± 0.1 °C and 12.0 ± 0.3 °C, respectively. Similar results were observed with the ICG concentration being increased to 20 μM (Figure S8B), in which the maximum temperature changes of solutions with free ICG and DI-NPs were 14.9 ± 0.2 °C and 19.0 ± 0.3 °C, respectively. The higher temperature changes exhibited by the DI-NPs systems can be attributed mainly to the red-shift in visible light absorption. As shown in Figure S8C, upon encapsulation in nanoparticles, the absorbance peak of ICG was appreciably shifted from

Table 1
Characteristics of DOX/ICG-loaded Nanoparticles.

Sample Code	D_h (nm)	PDI[a]	ZP[b] (mV)	E.E.[c] (wt. %)		L.C.[d] (wt. %)	
				DOX	ICG	DOX	ICG
Bare DI-NPs	50.8 ± 1.0	0.188 ± 0.035	−16.9 ± 1.6	66.7 ± 4.0	83.4 ± 7.0	5.6 ± 0.3	6.9 ± 0.6
CP2k-DI-NPs	52.0 ± 1.8	0.154 ± 0.057	−17.7 ± 1.5	63.8 ± 5.7	86.8 ± 3.6	4.6 ± 0.4	6.2 ± 0.3
CP5k-DI-NPs	54.1 ± 1.3	0.148 ± 0.030	−16.6 ± 0.2	66.8 ± 3.8	86.8 ± 3.5	4.8 ± 0.3	6.2 ± 0.3
CP10k-DI-NPs	57.7 ± 1.2	0.163 ± 0.012	−14.2 ± 0.3	66.6 ± 4.6	84.9 ± 7.8	4.7 ± 0.3	6.1 ± 0.6

[a] polydispersity index.
[b] Zeta potential.
[c] Loading efficiency.
[d] Loading content.

779 to 792 nm, resulting in higher photothermal efficiency than free ICG under 808 nm irradiation. Similar results have been reported elsewhere [56,57]. In addition, the ICG encapsulated in DI-NPs could form high ICG concentraion region, wihich upon irradiation colud lead to appreciable temperature increase due to low heat dissipation [57,58].

3.4. Cellular uptake

The cellular uptake of DI-NPs in MCF-7 and MCF-7/MDR cells was characterized by flow cytometry. Contrary to the data shown in Figure S9A in which MCF-7 cells treated with free DOX-HCl exhibited higher mean fluorescence intensity, the signal intensity of MCF-7/MDR cells treated with free DOX base was higher than that with free DOX-HCl (Fig. 2). This is attributed to the hydrophobic nature of DOX base that allows it to better associate with the cholesterol-rich lipid raft of MCF-7/MDR cells after being pumped out by lipid raft-bound P-gp [59,60]. It was also found that the mean DOX fluorescence intensities of the MCF7/MDR cell treated with DI-NPs were significantly higher than that with free DOX base. This phenomenon has been attributed to the binding of γ-PGA side chains on the surface of the nanoparticles to γ-glutamyl transpeptidase (γ-GGT), a membrane glycoprotein which modulates several physiological and pathological conditions for various cancer cell lines [61,62], leading to the enhanced endocytosis of DI-NPs [25]. The similar results were also observed for MCF-7 cells and other cancer cells (Figure S9), implying that the γ-PGA-based nanoparticles

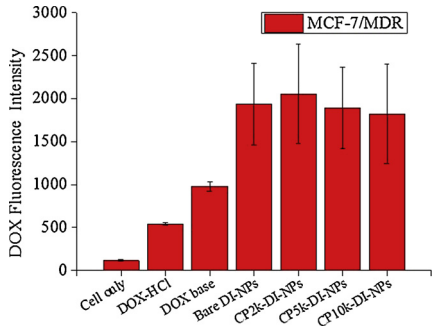

Fig. 2. Intracellular DOX fluorescence intensity in MCF-7/MDR cells incubated respectively with DOX-HCl, DOX base, bare DI-NPs, CP2k-DI-NPs, CP5k-DI-NPs, and CP10k-DI-NPs. (DOX concentration = 20 μM) for 6 h (n = 3).

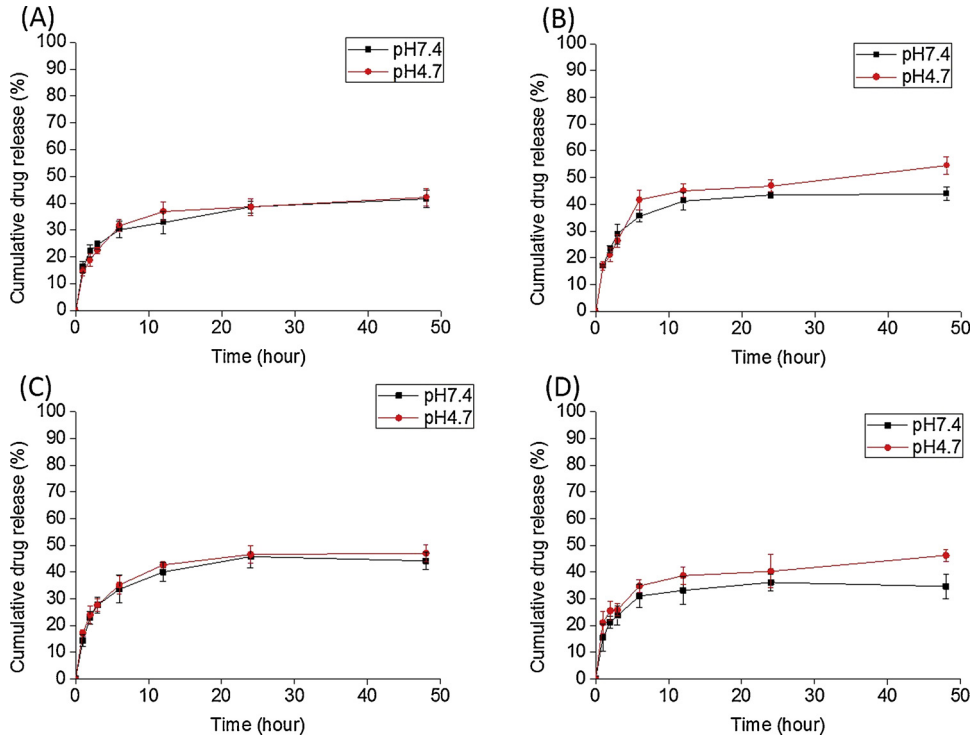

Fig. 1. Cumulative drug release profiles of DOX (base)-loaded (A) bare DI-NPs, (B) CP2k-DI-NPs, (C) CP5k-DI-NPs, and (D) CP10k-DI-NPs in buffered saline solutions of pH 7.4 (phosphate) and 4.7 (succinate) at 37 °C. (n = 3).

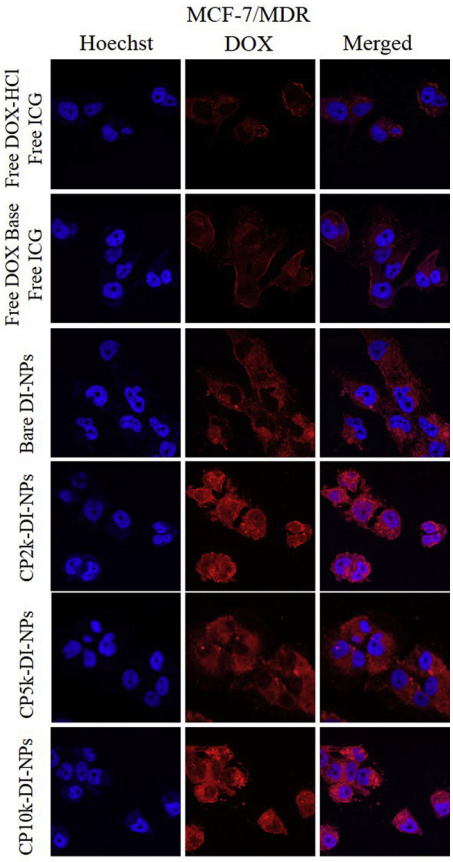

Fig. 3. LSCM images of MCF-7/MDR cells co-incubated respectively with free DOX-HCl/ICG, free DOX base/ICG, bare DI-NPs, CP2k-DI-NPs, CP5k-DI-NPs and CP10k-DI-NPs at 37 °C for 6 h with the DOX/ICG concentration of 20/20 μM. Cell nuclei were stained with Hoechst 33258.

developed in this study are well suited for the delivery of anticancer drugs to a variety of cancers.

To study the intracellular distribution of DOX in cancer cells after the NP uptake, MCF-7 and MDF-7/MDR cells were co-incubated, respectively, with DI-NPs for 6 h at 37 °C. Free DOX was also used as a control for comparison. As shown in Figure S10, significant accumulation of DOX in cell nuclei was observed for MCF-7 cells treated with free DOX-HCl and DI-NPs, consistent with the results of the flow cytometry study shown in Figure S9A. By contrast, the DOX signal in MCF-7 cells treated with DOX base was relatively low, most probably because the DOX while being in free base form could not effectively diffuse into cytoplasm or nuclei of cancer cells due to its low solubility in cell culture medium. For the DOX distribution in MCF-7/MDR cells, as shown in Fig. 3, both free DOX-HCl and DOX base barely accumulated within the nuclei of the MDR cells due to the drug resistance mechanism mediated by P-gp. Although the DOX species was found in the cytoplasm of MCF-7/MDR cells treated with bare DI-NPs, it was not observed in the nuclei, suggesting that DOX was effectively pumped out by the P-gp expressed on the nuclear membranes, leading to the decreased accumulation of DOX in the nuclei [63,64]. By contrast, DOX was found in both cytoplasm and nuclei of MCF-7/MDR cells treated with CP-DI-NPs, implying that the C-PEG could inhibit the activity of P-gp on cell membranes and nuclear membranes as reported by virtue of the change of membrane composition with the C-PEG being associated with the membranes [65]. It has been reported that the inhibitory effects of amphiphilic PEG adducts on the P-gp activity of MDR cancer cells can be ascribed to two different intracellular actions. Pluronic, a kind of PEG derived amphiphiles, acts on the reduction of drug efflux in close association with the ATP depletion by disturbance of mitochondria membranes and interference of ATP production [10]. By contrast, the inhibition of the membrane P-gp activity operated by lipid/PEG conjugates, such as TPGS and C-PEG, relies strongly on the association of the PEG adducts with cell membranes that alters both the membrane fluidity and the lipid composition of lipid rafts intimately related to the function of P-gp [7,66,67].

The photothermal effect of DI-NPs was assessed with the DI-NPs engulfed MCF-7/MDR cells being irradiated (808 nm, 10 min, 0.75 W/cm^2). As shown in Fig. 4, the appreciably enhanced DOX intensity was observed in the MCF-7/MDR cells receiving laser irradiation following DI-NP treatment than that without irradiation, indicating that laser irradiation could substantially promote the DOX release from DI-NPs internalized within MCF-7/MDR cells, and thus improve the therapeutic efficacy of chemotherapy.

3.5. Synergistic effect study

To estimate the synergistic therapeutic efficacy of the ICG-based photothermal therapy combined with DOX chemotherapy, the viability of MCF-7/MDR cells receiving DI-NPs-mediated single- and dual-modality therapy was determined by MTT assay. As shown in Fig. 5A, although statistically there is no significant difference in cell viability among all groups by chemotherapy treatment alone, the cell viability of MCF-7/MDR cells treated with C-PEG-DI-NPs at the DOX/ICG concentrations of 20/20 μM, ranging from 62.6% to 79.7%, was lower than those treated with free DOX/ICG and with bare DI-NPs, implying that the C-PEG-DI-NPs could reduce the MDR of cancer cells. The high cell viability of MCF-7/MDR cells after being treated, respectively, with free drug and various DI-NPs was partly ascribed to the low cytotoxicity of DOX base as compared to DOX-HCl (Figure S11A) due to the strong hydrophobic association with cell or nucleus membranes. Nevertheless, with the MCF-7 cancer cells (without MDR) being treated, the cell cytotoxicity was appreciable enhanced (Figure S11B) in comparison with the resistant cancer cells (Fig. 5A), elucidating the drug efflux effect of MCF-7/MDR cells that considerably reduced the chemotherapeutic efficacy.

In the in vitro photothermal therapy study, no significant difference in cell viability was observed for MCF-7/MDR cells treated with free ICG in concentration range 5~20 μM (Fig. 5B). This was attributed to low cellular uptake of free ICG by MCF-7/MDR cells and low photothermal effect of free ICG, with a maximum absorbance at 779 nm, yet irradiated at 808 nm, as described above. Besides, it has been reported that free ICG could be pumped out by the P-gp in MDR cells [68]. In contrast, the low cell viability of MCF-7/MDR cells treated with I-NPs at the ICG concentrations of 10 and 20 μM indicated profound thermal ablation against MCF-7/MDR cells by virtue of the efficient cellular internalization and accumulation of the γ-PGA-based nanoparticles in the MDR cells. Furthermore, the encapsulation of ICG in the I-NPs resulted in a red shift in the wavelength of maximum absorbance from 779 to 798 nm, leading to higher temperature elevation and thus higher photothermal therapeutic efficiency for MCF-7/MDR cells. Compared to the chemotherapy, the photothermal therapy exhibited superior therapeutic efficiency for MCF-7/MDR cells.

The cell viability of MCF-7/MDR cells treated with free DOX/ICG or DI-NPs under laser irradiation in combination therapy study is shown in Fig. 5C. Low cytotoxicity was observed for the groups treated with free ICG/DOX. In contrast, high cytotoxicity against MCF-7/MDR cells was observed for the groups treated with DI-NPs under irradiation. At the DOX/ICG concentrations of 10/10 μM and 20/20 μM, the cell viability for the groups treated with DI-NPs under irradiation, ranging from 4.7% to 13.9%, was significant lower than the groups treated with I-NPs under irradiation, ranging from 23.7% to 40.7%. This results indicated that photo-activation of the DI-NPs could not only induce hyperthermia ablation in cancer cells, but also prompt the release of DOX from nanoparticles due to the temperature increase in the microenvironment, demonstrating the therapeutic efficacy of the combination therapy

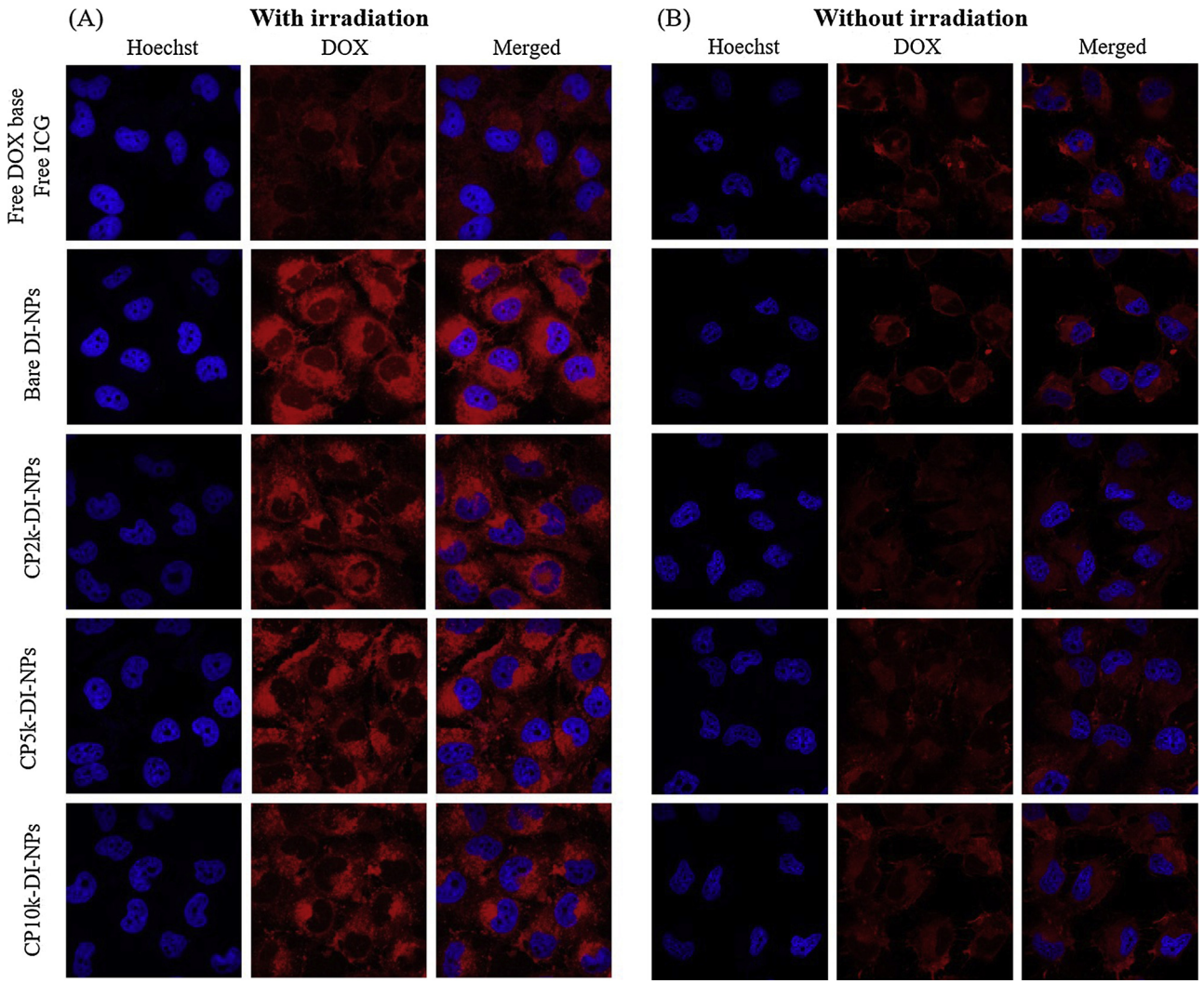

Fig. 4. LSCM images of MCF-7/MDR cells co-incubated with (A) free DOX/ICG, bare DI-NPs, CP2k-DI-NPs, CP5k-DI-NPs, or CP10k-DI-NPs at 37 °C for 6 h, then treated with 808 nm laser irradiation for 10 min and re-incubated at 37 °C for 6 h and (B) only DOX base/ICG, bare DI-NPs, CP2k-DI-NPs, CP5k-DI-NPs, or CP10k-DI-NPs at 37 °C for 12 h without laser irradiation. The final DOX/ICG concentrations are 20/20 μM. Cell nuclei were stained with Hoechst 33258.

against MDR cells with the DI-NPs.

The data of single therapy and combination therapy were analyzed with Compusyn using method [69,70]. The results are shown in Figure S12. The combination index (CI) of the group treated with free DOX/ICG was higher than 1, indicating that the dual free drug treatment exhibited an antagonistic effect. The CI of the group treated with DI-NPs was lower than 1, indicating that the DI-NPs under 808 nm irradiation displayed synergistic therapeutic efficacy, resulting from heat induced hyperthermia and DOX release, especially for CP2k-DI-NPs with high DOX/ICG concentrations.

3.6. Biodistribution

To examine the biodistribution of free drugs or DI-NPs by IVIS, ICG was used as a fluorescence probe in living bodies. As shown in Fig. 6A, the groups treated with free drugs exhibited low ICG intensity in the main organs and tumor most probably because the free ICG/DOX was easily metabolized and/or excreted, leading to a rapid clearance from living body. Slightly higher ICG signals at tumor site were observed in the group treated with bare DI-NPs, suggesting the enhanced metabolic stability and angiogenesis-induced tumor accumulation of the drugs-loaded NP delivery system. The groups treated with CP2k- and CP5k-DI-NPs displayed higher ICG intensity in the tumor sites than the groups treated with bare DI-NPs and CP10k-DI-NPs, implying that the C-PEG coating of the DI-NPs could promote the tumor EPR effects presumably by prolonging the NP residence in blood circulation [71,72] and inhibit the activity of P-gp of MCF-7/MDR cells and thus enhance drug accumulation with the appropriate lengths of PEG chain segments being employed. The low drug accumulation in tumor site for the group treated with CP10k-DI-NPs was probably caused by the reduced inhibitory activity of C-PEG10k on P-pg in association with the decreased aqueous mobility of the PEG chain segments with MW 10,000 g/mol. It should also be pointed out that the group treated with C-PEG-DI-NPs displayed lower ICG intensity in liver than the group treated with bare DI-NPs, except for the group treated with CP2k-DI-NPs. Since the accumulation of nanoparticles in liver has been attributed to the recognition of nanoparticles by liver's reticuloendothelial system (RES) [73], the reduced accumulation of C-PEG-DI-NPs in liver was caused primarily by the stealth effect provided by the hydrophilic PEG segments on the NP surfaces [74,75].

The amounts of ICG in major organs and tumor were quantitated. As shown in Fig. 6B, the amount of ICG accumulated in tumor for the group treated with CP2k-DI-NPs, 49.9 ± 20.6 ng, was at least twofold higher than those with CP5k-DI-NPs and CP10k-DI-NPs, 25.6 ± 21.5 ng and 4.6 ± 3.1 ng, respectively. Although the amount of ICG accumulated in liver for the group treated with CP2k-DI-NPs was

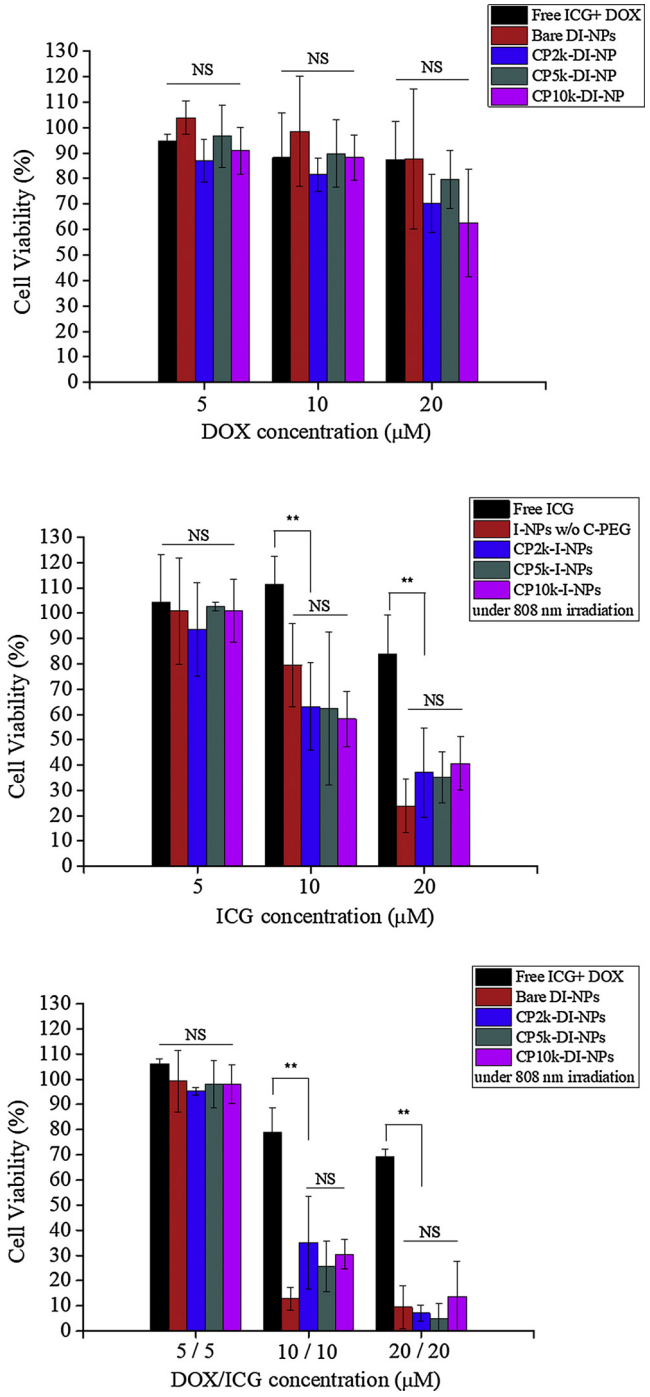

Fig. 5. Cell viability of MCF-7/MDR cells treated with (A) free DOX/ICG and DI-NPs, respectively, at 37 °C for 6 h and re-incubated at 37 °C for 48 h, (B) free ICG, I-NPs, respectively at 37 °C for 6 h, followed by laser irradiation at 808 nm for 10 min and re-incubated at 37 °C for 48 h, and (C) free DOX/ICG and DI-NPs and laser irradiation as described above. The DOX and ICG concentrations were in the range 5~20 μM. (n = 3).

also the highest among all the groups, the side effect of DI-NP accumulation in liver could be marginal as we have shown that DOX and ICG exhibited low cytotoxicity without irradiation in Fig. 5. The high tumor accumulation and synergistic therapeutic efficacy indicate that the CP2k-DI-NPs is a promising candidate for combination cancer therapy.

3.7. Tumor inhibition

To evaluate the *in vivo* antitumor efficacy of the proposed combination therapy, the mice bearing MCF-7/MDR tumor were administered intravenously with PBS, bare DI-NPs, and CP2k-DI-NPs. The tumor of mice was irradiated with 808 nm laser and the temperature change of tumor region was monitored by thermal camera. As shown in Figure S13A, the group treated with free dual drugs showed the lowest temperature increase duo to the low ICG accumulation in tumor sites. The mice treated with bare DI-NPs exhibited a limited temperature rise, only slightly higher than that treated with free dual drugs, because of the limited accumulation of bare DI-NPs in tumor due to its low colloidal stability and enhanced capture by the RES system. The highest temperature increase, from 37.4 ± 0.1 to 53.6 ± 5.9 °C, was observed in the group treated with CP2k-DI-NPs, indicating that CP2k-DI-NPs not only effectively extended the circulation half-life of ICG but also considerably increased its tumor accumulation compared to free drugs and bare DI-NPs, most likely due to its superior colloidal stability in blood stream. Higher temperature increase was observed for the tumor region under laser irradiation than the normal region in the infrared thermographic map as shown in Figure S13B. These results suggest that the thermal therapy can be performed selectively on tumor sites without the undesired thermal damage to normal tissues or organs, and is promising for clinical applications.

The cell apoptosis of tumors receiving various therapeutic formulations was identified by IHC staining of caspase-3 protein, an indicator for apoptosis pathway, in tumor sections. Fig. 7A shows that the DI-NPs groups without laser treatment exhibited a slight fluorescence signal, indicating that the NPs, CP2k-DI-NPs in particular, could induce the apoptosis of cancer cells by chemotherapy. Furthermore, the CP2k-DI-NPs groups with laser irradiation displayed an appreciably increase in cell apoptosis in tumor sites by combination therapy, which can be attributed to the facile accumulation of CP2k-DI-NPs in the tumor sites via EPR effects due to its colloid stability. Moreover, it has been reported that, with hyperthermia ablation, the local damages (including cell necrosis and apoptosis) of tumor tissues could result in expanded blood flow that further enhances accumulation and penetration of therapeutic nanoparticles into deep tumor tissues [76,77].

To estimate the antitumor efficiency of the combination therapy, the MCF-7/MDR tumor-bearing nude mice were treated with various formulations via tail vein injection. As shown in Fig. 7B and C and Figure S14, similar to the control group receiving only PBS, no reduction in tumor volume was observed for the group treated with free drugs and laser irradiation, indicating that the dual free drugs were effectively eliminated by liver or kidneys from blood stream and be excluded by P-gp on MCF-7/MDR cancer cells. While the tumor volume of the group treated with bare DI-NPs without laser irradiation, 507.6 ± 78.7 mm^3, was essentially identical to that of the PBS group, the tumor size of the group treated with bare DI-NPs and laser irradiation was reduced to 371.6 ± 30.8 mm^3. It can thus be postulated that the bare DI-NPs could slightly accumulate to tumor sites by EPR effects, leading to effective hyperthermia ablation against tumor by means of the photo-irradiation of ICG at 808 nm, even though the DOX base was pumped out by the MDR tumor cells. In the absence of photo-irradiation, the tumor volume of the group treated with CP2k-DI-NPs, 476.3 ± 54.1 mm^3, was slightly smaller than that of the group receiving bare DI-NPs, implying that the coating with C-PEG renders the NPs of improved colloid stability and thus increased tumor accumulation via EPR effects in comparison with bare DI-NPs. The C-PEG chain segments released from C-PEG-DI-NPs can inhibit the activity of P-gp on MDR cancer cells and further increase the chemotherapy efficacy of CP2k-DI-NPs. Upon laser irradiation, the tumor volume of the group treated with CP2k-DI-NPs was further reduced to 124.4 ± 22.1 mm^3, attesting to the efficacy of the proposed combination therapy against MDR cancer cells. In contrast with that of the groups treated with free drug and bare DI-NPs with laser, the H&E stained tumor sections of the

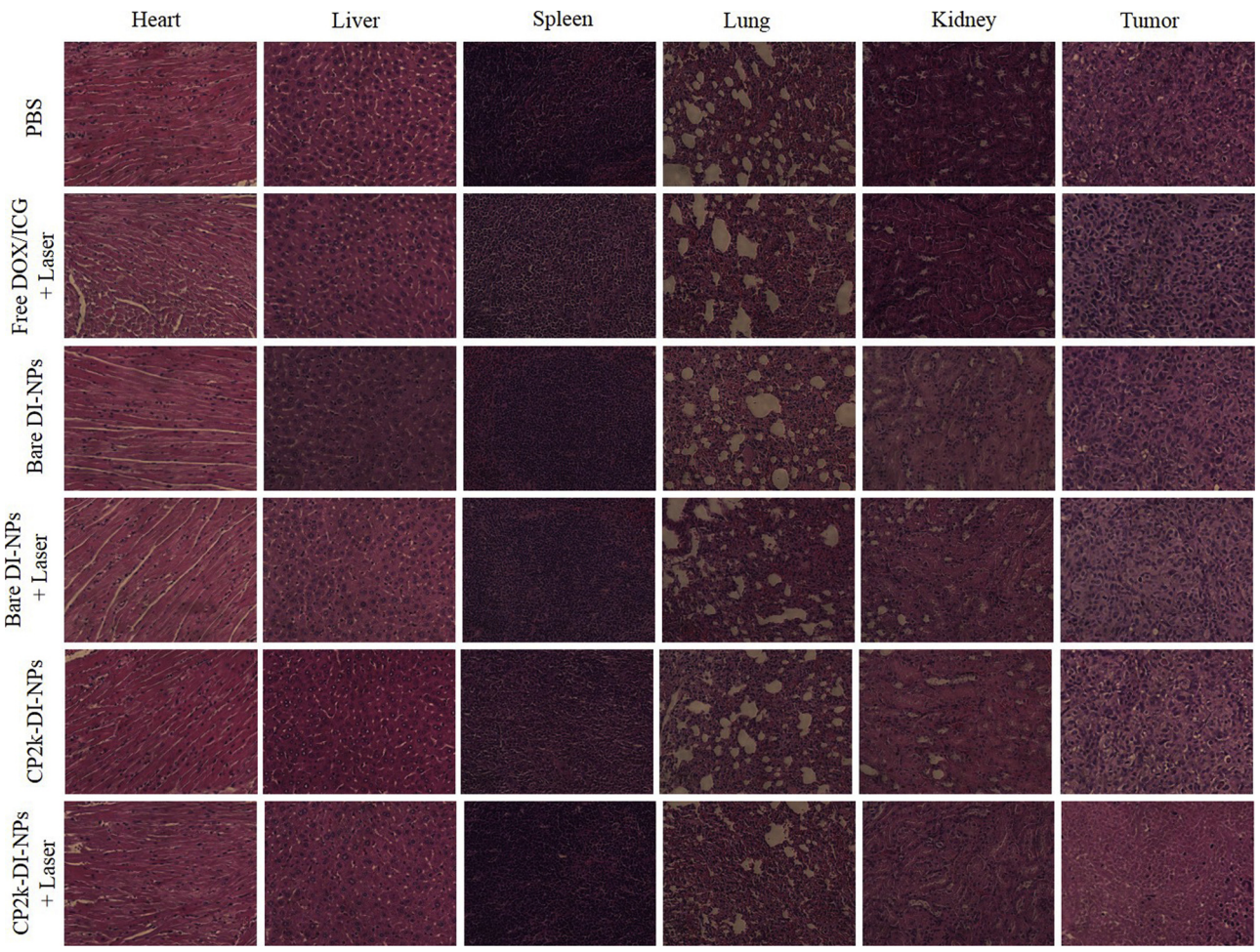

Fig. 6. ICG accumulation in major organs and tumors after the administration of free DOX base/ICG or DI-NPs. (A) The IVIS images of *ex vivo* organs and tumors. (B) ICG amounts in the organs and tumors. The images were taken 24 h post-DOX/ICG administration via tail vein injection. (n = 3).

group treated with CP2k-DI-NPs and laser irradiation exhibited significant reduction in the number of nuclei with enlarged apoptosis region (Figure S15).

To assess the side effects of the combination therapy, body weight of each mouse was also recorded after the administration of various formulations. As shown in Figure S16, no significant variation in body weight during the study was observed for all formulations, indicating that the DI-NPs did not induce specific toxicity for living bodies. Furthermore, as shown in Figure S15, no damage in the normal tissues of major organs was observed in the H & E staining for all formulations. These results indicate that photothermal/chemo combination therapy of CP2k-DI-NPs has superior anti-MDR tumor capability for clinical application with reduced side effects for normal organs.

4. Conclusions

To improve the efficacy of MDR tumor treatment by combination (photothermal/chemo) therapy, the polymeric nanoparticles based upon γ-PGA-g-PLGA coated with C-PEG were developed in this work to enhance the intracellular DOX/ICG level in the MDR breast tumor. The C-PEG-coated DI-NPs exhibited the high colloidal stability in cell culture medium and had an ideal particles size for tumor accumulation via EPR effects. The CP2k-DI-NPs showed the best cellular uptake by MCF-7/MDR cancer cells among other DI-NP formulations, confirming that C-PEG with an appropriate PEG chain length (2000 g/mol) can inhibit the activity of P-gp on the MCF-7/MDR cells meanwhile γ-PGA shells located on NP surfaces induced the cellular uptake via γ-PGA receptor-mediated endocytosis. With the combination therapy being applied, the photothermal therapy of DI-NPs can not only induce cancer cell death by thermal ablation but also enhance DOX release from the NPs, achieving synergistic therapeutic efficacy for cancer therapy in depressing the proliferation of MCF-7/MDR cells in vitro. The ex vivo biodistribution study indicated an enhanced accumulation of CP2k-DI-NPs in tumor owing to the profound EPR effects by prolonging the NP residence in blood circulation. The in vivo tumor inhibition evaluation also clearly demonstrated superior anti-MDR tumor efficacy with negligible tissue damage to major organs by the combination treatment of CP2k-DI-NPs and laser irradiation. It can be concluded that CP2k-DI-NPs are a promising drug delivery system for improving the efficacy of combination therapy against MDR tumors.

Disclosure

The authors report no conflicts of interest in this work.

Acknowledgments

This work is supported by the Ministry of Science and Technology (MOST106-2627-M-007-002-), National Tsing Hua University (107Q2521E1) and Hsinchu Mackay Memorial Hospital (MMH-TH-10702), Taiwan.

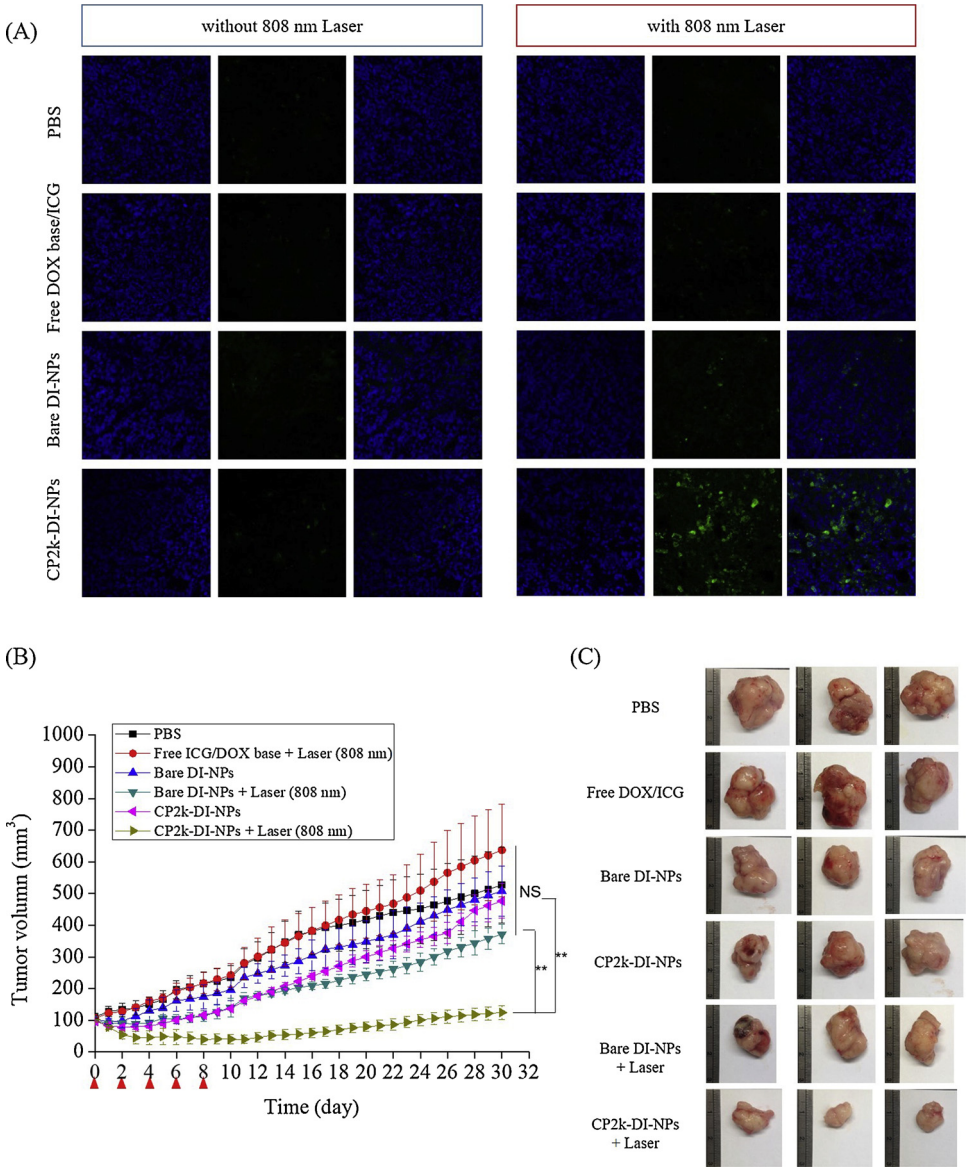

Fig. 7. (A) IHC-identified apoptosis of cancer cells from tumor sections. (Caspase-3 was stained in green and nuclei in blue). (B) *in vivo* antitumor effect of free DOX/ICG and DI-NPs on Balb/c nude mice bearing MCF-7/MDR tumors with and without photo-irradiation at 808 nm (0.75 W/cm^2) for 10 min. (C) *Ex vivo* tumor images from the groups receiving free DOX/ICG and DI-NPs with and without photo-irradiation. The scale bar is 3 cm. (n = 3) (For interpretation of the references to colour in this figure legend, the reader is referred to the web version of this article).

Appendix A. Supplementary data

Supplementary material related to this article can be found, in the online version, at doi:https://doi.org/10.1016/j.colsurfb.2019.02.001.

References

[1] E.M. Leslie, R.G. Deeley, S.P. Cole, Multidrug resistance proteins: role of P-glycoprotein, MRP1, MRP2, and BCRP (ABCG2) in tissue defense, Toxicol. Appl. Pharmacol. 204 (2005) 216–237.
[2] A. van Helvoort, A.J. Smith, H. Sprong, I. Fritzsche, A.H. Schinkel, P. Borst, G. van Meer, MDR1 P-glycoprotein is a lipid translocase of broad specificity, while MDR3 P-glycoprotein specifically translocates phosphatidylcholine, Cell 87 (1996) 507–517.
[3] M.M. van den Heuvel-Eibrink, P. Sonneveld, R. Pieters, The prognostic significance of membrane transport-associated multidrug resistance (MDR) proteins in leukemia, Int. J. Clin. Pharmacol. Ther. 38 (2000) 94–110.
[4] X.R. Song, Y. Zheng, G. He, L. Yang, Y.F. Luo, Z.Y. He, S.Z. Li, J.M. Li, S. Yu, X. Luo, S.X. Hou, Y.Q. Wei, Development of PLGA nanoparticles simultaneously loaded with vincristine and verapamil for treatment of hepatocellular carcinoma, J. Pharm. Sci. 99 (2010) 4874–4879.
[5] X. Duan, J. Xiao, Q. Yin, Z. Zhang, H. Yu, S. Mao, Y. Li, Smart pH-sensitive and temporal-controlled polymeric micelles for effective combination therapy of doxorubicin and disulfiram, ACS Nano 7 (2013) 5858–5869.
[6] H. Wu, W.N. Hait, J.M. Yang, Small interfering RNA-induced suppression of MDR1 (P-glycoprotein) restores sensitivity to multidrug-resistant cancer cells, Cancer Res. 63 (2003) 1515–1519.
[7] E.M. Collnot, C. Baldes, M.F. Wempe, R. Kappl, J. Huttermann, J.A. Hyatt, K.J. Edgar, U.F. Schaefer, C.M. Lehr, Mechanism of inhibition of P-glycoprotein mediated efflux by vitamin E TPGS: influence on ATPase activity and membrane fluidity, Mol. Pharm. 4 (2007) 465–474.
[8] J.L. Tang, Y.J. Wang, D. Wang, Y.H. Wang, Z.H. Xu, K. Racette, F. Liu, Key structure of brij for overcoming multidrug resistance in cancer, Biomacromolecules 14 (2013) 424–430.
[9] Y. Luo, D.W. Chen, L.X. Ren, X.L. Zhao, J. Qin, Solid lipid nanoparticles for enhancing vinpocetine's oral bioavailability, J. Control. Release 114 (2006) 53–59.
[10] T. Minko, E.V. Batrakova, S. Li, Y.L. Li, R.I. Pakunlu, V.Y. Alakhov, A.V. Kabanov, Pluronic block copolymers alter apoptotic signal transduction of doxorubicin in drug-resistant cancer cells, J. Control. Release 105 (2005) 269–278.
[11] M.J. Shieh, C.Y. Hsu, L.Y. Huang, H.Y. Chen, F.H. Huang, P.S. Lai, Reversal of doxorubicin-resistance by multifunctional nanoparticles in MCF-7/ADR cells, J. Control. Release 152 (2011) 418–425.
[12] J. Lipman, I. Jardine, C. Roos, L. Dreosti, Intravenous Calcium chloride as an antidote to verapamil-induced hypotension, Intens. Care Med. 8 (1982) 55–57.
[13] A. Berdeaux, R. Coutte, J. Giudicelli, J. Boissier, Effects of verapamil on regional myocardial blood flow and ST segment. Role of the induced bradycardia, Eur. J.

Pharmacol. 39 (1976) 287–294.
[14] H. Meng, M. Liong, T. Xia, Z. Li, Z. Ji, J.I. Zink, A.E. Nel, Engineered design of mesoporous silica nanoparticles to deliver doxorubicin and P-glycoprotein siRNA to overcome drug resistance in a cancer cell line, ACS Nano 4 (2010) 4539–4550.
[15] G. Navarro, R.R. Sawant, S. Biswas, S. Essex, C. Tros de Ilarduya, V.P. Torchilin, P-glycoprotein silencing with siRNA delivered by DOPE-modified PEI overcomes doxorubicin resistance in breast cancer cells, Nanomedicine 7 (2012) 65–78.
[16] L. Parhamifar, A.K. Larsen, A.C. Hunter, T.L. Andresen, S.M. Moghimi, Polycation cytotoxicity: a delicate matter for nucleic acid therapy-focus on polyethylenimine, Soft Matter 6 (2010) 4001–4009.
[17] S.P. Hong, P.R. Leroueil, E.K. Janus, J.L. Peters, M.M. Kober, M.T. Islam, B.G. Orr, J.R. Baker, M.M.B. Holl, Interaction of polycationic polymers with supported lipid bilayers and cells: nanoscale hole formation and enhanced membrane permeability, Bioconjug. Chem. 17 (2006) 728–734.
[18] K.B. Ghaghada, J. Saul, J.V. Natarajan, R.V. Bellamkonda, A.V. Annapragada, Folate targeting of drug carriers: a mathematical model, J. Control. Release 104 (2005) 113–128.
[19] F. Danhier, O. Feron, V. Preat, To exploit the tumor microenvironment: passive and active tumor targeting of nanocarriers for anti-cancer drug delivery, J. Control. Release 148 (2010) 135–146.
[20] E.S. Lee, H.J. Shin, K. Na, Y.H. Bae, Poly(L-histidine)-PEG block copolymer micelles and pH-induced destabilization, J. Control. Release 90 (2003) 363–374.
[21] L.Y. Zeng, Y.W. Pan, Y. Tian, X. Wang, W.Z. Ren, S.J. Wang, G.M. Lu, A.G. Wu, Doxorubicin-loaded NaYF4:Yb/Tm-TiO2 inorganic photosensitizers for NIR-triggered photodynamic therapy and enhanced chemotherapy in drug-resistant breast cancers, Biomaterials 57 (2015) 93–106.
[22] Y. Tang, T. Lei, R. Manchanda, A. Nagesetti, A. Fernandez-Fernandez, S. Srinivasan, A.J. McGoron, Simultaneous delivery of chemotherapeutic and thermal-optical agents to cancer cells by a polymeric (PLGA) nanocarrier: an in vitro study, Pharm. Res. 27 (2010) 2242–2253.
[23] W.C. Huang, S.H. Chen, W.H. Chiang, C.W. Huang, C.L. Lo, C.S. Chern, H.C. Chiu, Tumor microenvironment-responsive nanoparticle delivery of chemotherapy for enhanced selective cellular uptake and transportation within tumor, Biomacromolecules 17 (2016) 3883–3892.
[24] S. Abbad, C. Wang, A.Y. Waddad, H. Lv, J. Zhou, Preparation, in vitro and in vivo evaluation of polymeric nanoparticles based on hyaluronic acid-poly(butyl cyanoacrylate) and D-alpha-tocopheryl polyethylene glycol 1000 succinate for tumor-targeted delivery of morin hydrate, Int. J. Nanomed. 10 (2015) 305–320.
[25] S.F. Peng, M.T. Tseng, Y.C. Ho, M.C. Wei, Z.X. Liao, H.W. Sung, Mechanisms of cellular uptake and intracellular trafficking with chitosan/DNA/poly(gamma-glutamic acid) complexes as a gene delivery vector, Biomaterials 32 (2011) 239–248.
[26] E.S. Lee, K. Na, Y.H. Bae, Doxorubicin loaded pH-sensitive polymeric micelles for reversal of resistant MCF-7 tumor, J. Control. Release 103 (2005) 405–418.
[27] R. Feng, Z. Song, G. Zhai, Preparation and in vivo pharmacokinetics of curcumin-loaded PCL-PEG-PCL triblock copolymeric nanoparticles, Int. J. Nanomed. 7 (2012) 4089–4098.
[28] T. Ramasamy, H.B. Ruttala, N. Chitrapriya, B.K. Poudal, J.Y. Choi, S.T. Kim, Y.S. Youn, S.K. Ku, H.G. Choi, C.S. Yong, J.O. Kim, Engineering of cell microenvironment-responsive polypeptide nanovehicle co-encapsulating a synergistic combination of small molecules for effective chemotherapy in solid tumors, Acta Biomater. 48 (2017) 131–143.
[29] H.B. Ruttala, N. Chitrapriya, K. Kaliraj, T. Ramasamy, W.H. Shin, J.H. Jeong, J.R. Kim, S.K. Ku, H.G. Choi, C.S. Yong, J.O. Kim, Facile construction of bioreducible crosslinked polypeptide micelles for enhanced cancer combination therapy, Acta Biomater. 63 (2017) 135–149.
[30] T. Ramasamy, H.B. Ruttala, J.Y. Choi, T.H. Tran, J.H. Kim, S.K. Ku, H.G. Choi, C.S. Yong, J.O. Kim, Engineering of a lipid-polymer nanoarchitectural platform for highly effective combination therapy of doxorubicin and irinotecan, Chem. Commun. 51 (2015) 5758–5761.
[31] C.C. Hung, W.C. Huang, Y.W. Lin, T.W. Yu, H.H. Chen, S.C. Lin, W.H. Chiang, H.C. Chiu, Active tumor permeation and uptake of surface charge-switchable theranostic nanoparticles for imaging-guided photothermal/chemo combinatorial therapy, Theranostics 6 (2016) 302–317.
[32] T. Ramasamy, Z.S. Haidar, T.H. Tran, J.Y. Choi, J.H. Jeong, B.S. Shin, H.G. Choi, C.S. Yong, J.O. Kim, Layer-by-layer assembly of liposomal nanoparticles with PEGylated polyelectrolytes enhances systemic delivery of multiple anticancer drugs, Acta Biomater. 10 (2014) 5116–5127.
[33] W.T. Li, J.R. Peng, L.W. Tan, J. Wu, K. Shi, Y. Qu, X.W. Wei, Z.Y. Qian, Mild photothermal therapy/photodynamic therapy/chemotherapy of breast cancer by Lyp-1 modified Docetaxel/IR820 Co-loaded micelles, Biomaterials 106 (2016) 119–133.
[34] T.K. Jain, J. Richey, M. Strand, D.L. Leslie-Pelecky, C.A. Flask, V. Labhasetwar, Magnetic nanoparticles with dual functional properties: drug delivery and magnetic resonance imaging, Biomaterials 29 (2008) 4012–4021.
[35] J. Kim, H.S. Kim, N. Lee, T. Kim, H. Kim, T. Yu, I.C. Song, W.K. Moon, T. Hyeon, Multifunctional uniform nanoparticles composed of a magnetite nanocrystal core and a mesoporous silica shell for magnetic resonance and fluorescence imaging and for drug delivery, Angew. Chem. Int. Ed. Engl. 47 (2008) 8438–8441.
[36] T. Ramasamy, H.B. Ruttala, B. Gupta, B.K. Poudel, H.G. Choi, C.S. Yong, J.O. Kim, Smart chemistry-based nanosized drug delivery systems for systemic applications: a comprehensive review, J. Control. Release 258 (2017) 226–253.
[37] X. Huang, I.H. El-Sayed, W. Qian, M.A. El-Sayed, Cancer cell imaging and photothermal therapy in the near-infrared region by using gold nanorods, J. Am. Chem. Soc. 128 (2006) 2115–2120.
[38] J.T. Robinson, S.M. Tabakman, Y. Liang, H. Wang, H.S. Casalongue, D. Vinh, H. Dai, Ultrasmall reduced graphene oxide with high near-infrared absorbance for photothermal therapy, J. Am. Chem. Soc. 133 (2011) 6825–6831.
[39] T. Ramasamy, H.B. Ruttala, P. Sundaramoorthy, B.K. Poudel, Y.S. Youn, S.K. Ku, H.G. Choi, C.S. Yong, J.O. Kim, Multimodal selenium nanoshell-capped Au@mSiO(2) nanoplatform for NIR-responsive chemo-photothermal therapy against metastatic breast cancer, NPG Asia Mater. 10 (2018) 197–216.
[40] M. Zheng, C. Yue, Y. Ma, P. Gong, P. Zhao, C. Zheng, Z. Sheng, P. Zhang, Z. Wang, L. Cai, Single-step assembly of DOX/ICG loaded lipid-polymer nanoparticles for highly effective chemo-photothermal combination therapy, ACS Nano 7 (2013) 2056–2067.
[41] H. Xu, Y. Deng, D. Chen, W. Hong, Y. Lu, X. Dong, Esterase-catalyzed dePEGylation of pH-sensitive vesicles modified with cleavable PEG-lipid derivatives, J. Control. Release 130 (2008) 238–245.
[42] J.M. Harris, E.C. Struck, M.G. Case, M.S. Paley, J.M. Vanalstine, D.E. Brooks, Synthesis and characterization of poly(ethylene glycol) derivatives, J. Polym. Sci.: Polym. Chem. Ed. 22 (1984) 341–352.
[43] V.A. Sethuraman, Y.H. Bae, TAT peptide-based micelle system for potential active targeting of anti-cancer agents to acidic solid tumors, J. Control. Release 118 (2007) 216–224.
[44] M.V. Berridge, A.S. Tan, Characterization of the Cellular Reduction of 3-(4,5-Dimethylthiazol-2-Yl)-2,5-Diphenyltetrazolium Bromide (Mtt) - Subcellular-Localization, Substrate Dependence, and Involvement of Mitochondrial Electron-Transport in Mtt Reduction, Arch. Biochem. Biophys. 303 (1993) 474–482.
[45] C.Y. Hsieh, R.C. Santell, S.Z. Haslam, W.G. Helferich, Estrogenic effects of genistein on the growth of estrogen receptor-positive human breast cancer (MCF-7) cells in vitro and in vivo, Cancer Res. 58 (1998) 3833–3838.
[46] J.L. Ruan, N.L. Tulloch, V. Muskheli, E.E. Genova, P.D. Mariner, K.S. Anseth, C.E. Murry, An improved cryosection method for polyethylene glycol hydrogels used in tissue engineering, Tissue Eng. Part C Methods 19 (2013) 794–801.
[47] J. Xie, C. Xu, N. Kohler, Y. Hou, S. Sun, Controlled PEGylation of monodisperse Fe3O4 nanoparticles for reduced non-specific uptake by macrophage cells, Adv. Mater. 19 (2007) 3163–3166.
[48] P.F. Zhao, M.B. Zheng, C.X. Yue, Z.Y. Luo, P. Gong, G.H. Gao, Z.H. Sheng, C.F. Zheng, L.T. Cai, Improving drug accumulation and photothermal efficacy in tumor depending on size of ICG loaded lipid-polymer nanoparticles, Biomaterials 35 (2014) 6037–6046.
[49] E. Frohlich, The role of surface charge in cellular uptake and cytotoxicity of medical nanoparticles, Int. J. Nanomed. Nanosurg. 7 (2012) 5577–5591.
[50] F.M. Kievit, F.Y. Wang, C. Fang, H. Mok, K. Wang, J.R. Silber, R.G. Ellenbogen, M.Q. Zhang, Doxorubicin loaded iron oxide nanoparticles overcome multidrug resistance in cancer in vitro, J. Control. Release 152 (2011) 76–83.
[51] Q. Zhang, X.L. Wang, P.Z. Li, K.T. Nguyen, X.J. Wang, Z. Luo, H.C. Zhang, N.S. Tan, Y.L. Zhao, Biocompatible, uniform, and redispersible mesoporous silica nanoparticles for cancer-targeted drug delivery in vivo, Adv. Funct. Mater. 24 (2014) 2450–2461.
[52] Y. Yu, C.K. Chen, W.C. Law, H. Sun, P.N. Prasad, C. Cheng, A degradable brush polymer-drug conjugate for pH-responsive release of doxorubicin, Polym. Chem. 6 (2015) 953–961.
[53] T. Iijima, T. Aoyagi, Y. Iwao, J. Masuda, M. Fuse, N. Kobayashi, H. Sankawa, Cardiac output and circulating blood volume analysis by pulse dye-densitometry, J. Clin. Monitor 13 (1997) 81–89.
[54] C.M. Leevy, F. Smith, J. Longueville, G. Paumgartner, M.M. Howard, Indocyanine green clearance as a test for hepatic function, J. Am. Med. Assoc. 200 (1967) 236–240.
[55] S. Mordon, J.M. Devoisselle, S. Soulie-Begu, T. Desmettre, Indocyanine green: physicochemical factors affecting its fluorescence in vivo, Microvasc. Res. 55 (1998) 146–152.
[56] Z.H. Wan, H.J. Mao, M. Guo, Y.L. Li, A.J. Zhu, H. Yang, H. He, J.K. Shen, L.J. Zhou, Z. Jiang, C.C. Ge, X.Y. Chen, X.L. Yang, G. Liu, H.B. Chen, Highly efficient hierarchical micelles integrating photothermal therapy and singlet oxygen-synergized chemotherapy for cancer eradication, Theranostics 4 (2014) 399–411.
[57] M.B. Zheng, P.F. Zhao, Z.Y. Luo, P. Gong, C.F. Zheng, P.F. Zhang, C.X. Yue, D.Y. Gao, Y.F. Ma, L.T. Cai, Robust ICG theranostic nanoparticles for folate targeted cancer imaging and highly effective photothermal therapy, ACS Appl. Mater. Interfaces 6 (2014) 6709–6716.
[58] M.B. Zheng, C.X. Yue, Y.F. Ma, P. Gong, P.F. Zhao, C.F. Zheng, Z.H. Sheng, P.F. Zhang, Z.H. Wang, L.T. Cai, Single-step assembly of DOX/ICG loaded lipid-polymer nanoparticles for highly effective chemo-photothermal combination therapy, ACS Nano 7 (2013) 2056–2067.
[59] M.A. Ghetie, R. Marches, S. Kufert, E.S. Vitetta, An anti-CD19 antibody inhibits the interaction between P-glycoprotein (P-gp) and CD 19, causes P-gp to translocate out of lipid rafts, and chemosensitizes a multidrug-resistant (NMR) lymphoma cell line, Blood 104 (2004) 178–183.
[60] S. Orlowski, S. Martin, A. Escargueil, P-glycoprotein and' lipid rafts': some ambiguous mutual relationships (floating on them, building them or meeting them by chance?), Cell. Mol. Life Sci. 63 (2006) 1038–1059.
[61] S. Daubeuf, M.J. Accaoui, I. Pettersen, N.E. Huseby, A. Visvikis, M.M. Galteau, Differential regulation of gamma-glutamyltransferase mRNAs in four human tumour cell lines, Biochim. Biophys. Acta Gen. Subj. 1568 (2001) 67–73.
[62] L. Wasserman, J. Nordenberg, E. Beery, A.A. Deutsch, A. Novogrodsky, Differential-effects of sodium-butyrate and dimethylsulfoxide on gamma-glutamyl-transferase transpeptidase and alkaline-phosphatase activities in MCF-7 breast-cancer cells, Exp. Cell Biol. 55 (1987) 189–193.
[63] W. Szaflarski, P. Sujka-Kordowska, R. Januchowski, K. Wojtowicz, M. Andrzejewska, M. Nowicki, M. Zabel, Nuclear localization of P-glycoprotein is responsible for protection of the nucleus from doxorubicin in the resistant LoVo cell line, Biomed. Pharmacother. 67 (2013) 497–502.

[64] Y. Chao, Y. Liang, G. Fang, H. He, Q. Yao, H. Xu, Y. Chen, X. Tang, Biodegradable polymersomes as nanocarriers for doxorubicin hydrochloride: enhanced cytotoxicity in MCF-7/ADR cells and prolonged blood circulation, Pharm. Res. 34 (2017) 610–618.
[65] H.H. Chen, W.C. Huang, W.H. Chiang, T.I. Liu, M.Y. Shen, Y.H. Hsu, S.C. Lin, H.C. Chiu, pH-Responsive therapeutic solid lipid nanoparticles for reducing P-glycoprotein-mediated drug efflux of multidrug resistant cancer cells, Int. J. Nanomed. 10 (2015) 5035–5048.
[66] S.M. dos Santos, C.C. Weber, C. Franke, W.E. Muller, G.P. Eckert, Cholesterol: coupling between membrane microenvironment and ABC transporter activity, Biochem. Biophys. Res. Commun. 354 (2007) 216–221.
[67] J. Zastre, J.K. Jackson, W. Wong, H.M. Burt, Methoxypolyethylene glycol-block-polycaprolactone diblock copolymers reduce P-glycoprotein efflux in the absence of a membrane fluidization effect while stimulating P-glycoprotein ATPase activity, J. Pharm. Sci. 96 (2007) 864–875.
[68] E. Portnoy, M. Gurina, S. Magdassi, S. Eyal, Evaluation of the near infrared compound indocyanine green as a probe substrate of p-glycoprotein, Mol. Pharmacol. 9 (2012) 3595–3601.
[69] N. Zhang, J.N. Fu, T.C. Chou, Synergistic combination of microtubule targeting anticancer fludelone with cytoprotective panaxytriol derived from panax ginseng against MX-1 cells in vitro: experimental design and data analysis using the combination index method, Am. J. Cancer Res. 6 (2016) 97–104.
[70] T.C. Chou, P. Talalay, Quantitative-analysis of dose-effect relationships - the combined effects of multiple-drugs or enzyme-inhibitors, Adv. Enzyme Regul. 22 (1984) 27–55.
[71] P.J. Photos, L. Bacakova, B. Discher, F.S. Bates, D.E. Discher, Polymer vesicles in vivo: correlations with PEG molecular weight, J. Control. Release 90 (2003) 323–334.
[72] B. Shi, C. Fang, Y.Y. Pei, Stealth PEG-PHDCA niosomes: effects of chain length of PEG and particle size on niosomes surface properties, in vitro drug release, phagocytic uptake, in vivo pharmacokinetics and antitumor activity, J. Pharm. Sci. 95 (2006) 1873–1887.
[73] S.D. Li, L. Huang, Nanoparticles evading the reticuloendothelial system: role of the supported bilayer, Biochim. Biophys. Acta 1788 (2009) 2259–2266.
[74] S.D. Li, L. Huang, Stealth nanoparticles: high density but sheddable PEG is a key for tumor targeting, J. Control. Release 145 (2010) 178–181.
[75] G. Pasut, D. Paolino, C. Celia, A. Mero, A.S. Joseph, J. Wolfram, D. Cosco, O. Schiavon, H. Shen, M. Fresta, Polyethylene glycol (PEG)-dendron phospholipids as innovative constructs for the preparation of super stealth liposomes for anticancer therapy, J. Control. Release 199 (2015) 106–113.
[76] D.K. Kirui, E.J. Koay, X.J. Guo, V. Cristini, H.F. Shen, M. Ferrari, Tumor vascular permeabilization using localized mild hyperthermia to improve macromolecule transport, Nanomedicine 10 (2014) 1487–1496.
[77] K. Yang, H. Xu, L. Cheng, C.Y. Sun, J. Wang, Z. Liu, In vitro and in vivo near-infrared photothermal therapy of cancer using polypyrrole organic nanoparticles, Adv. Mater. 24 (2012) 5586–5592.